The Chromospheres of G-type Ib Supergiants

Alex Lobel & Andrea K. Dupree

alobel@cfa.harvard.edu, adupree@cfa.harvard.edu

Smithsonian Astrophysical Observatory, 60 Garden St., Cambridge MA

Poster paper #44.15 presented at the 197th AAS Meeting, Jan. 9 2001, San Diego CA

Summary

This preliminary study of the detailed chromospheric conditions of G-type Ib-supergiants provides a foundation for atmospheric models, complementing *STIS* and *FUSE* surveys of cool stars.

We model and compare the chromospheric conditions and dynamics of ϵ Gem (G8 Ib) and Betelgeuse (M2 Iab), based on high-resolution STIS spectra. We discuss a comparison of optical and near-UV high-dispersion Utrecht Echelle Spectrograph (William Herschel Telescope), and *SOFIN* (Nordic Optical Telescope) echelle spectra of α Aqr (G2 Ib), 9 Peg (G5 Ib), and ϵ Gem with the Ia-supergiant HD 179821 (G2-G5). The latter has recently been proposed as a post-AGB star instead of a population I massive supergiant, for which we do not detect chromospheric emission in Ca II H & K.

The three Ib-supergiants reveal much stronger Hα absorption

lines than HD 179821, while the core intensities of Hβ and Hδ (showing broad damping line wings) in α Aqr, 9 Peg, and HD 179821 are similar. The Hα pro£le of HD 179821 has a weak absorption core with satellite emission, typically formed in a supersonic expanding wind. This is regularly observed in very luminous cool pulsating super- and hypergiants of the ρ Cas-type (F2-G Ia^{+}), which lack H & K emission.

Our spectral synthesis shows that the Hα absorption in late G Ib-supergiants is strongly enhanced due to chromospheric excitation, whereas the higher Balmer lines are mainly of photospheric origin. This £nding is parallel to the chromospheric nature of Hα absorption in Betelgeuse, recently discussed by Lobel & Dupree (ApJ, 2000, 545, 454).

This research is supported in part by STScI grant to the SAO.

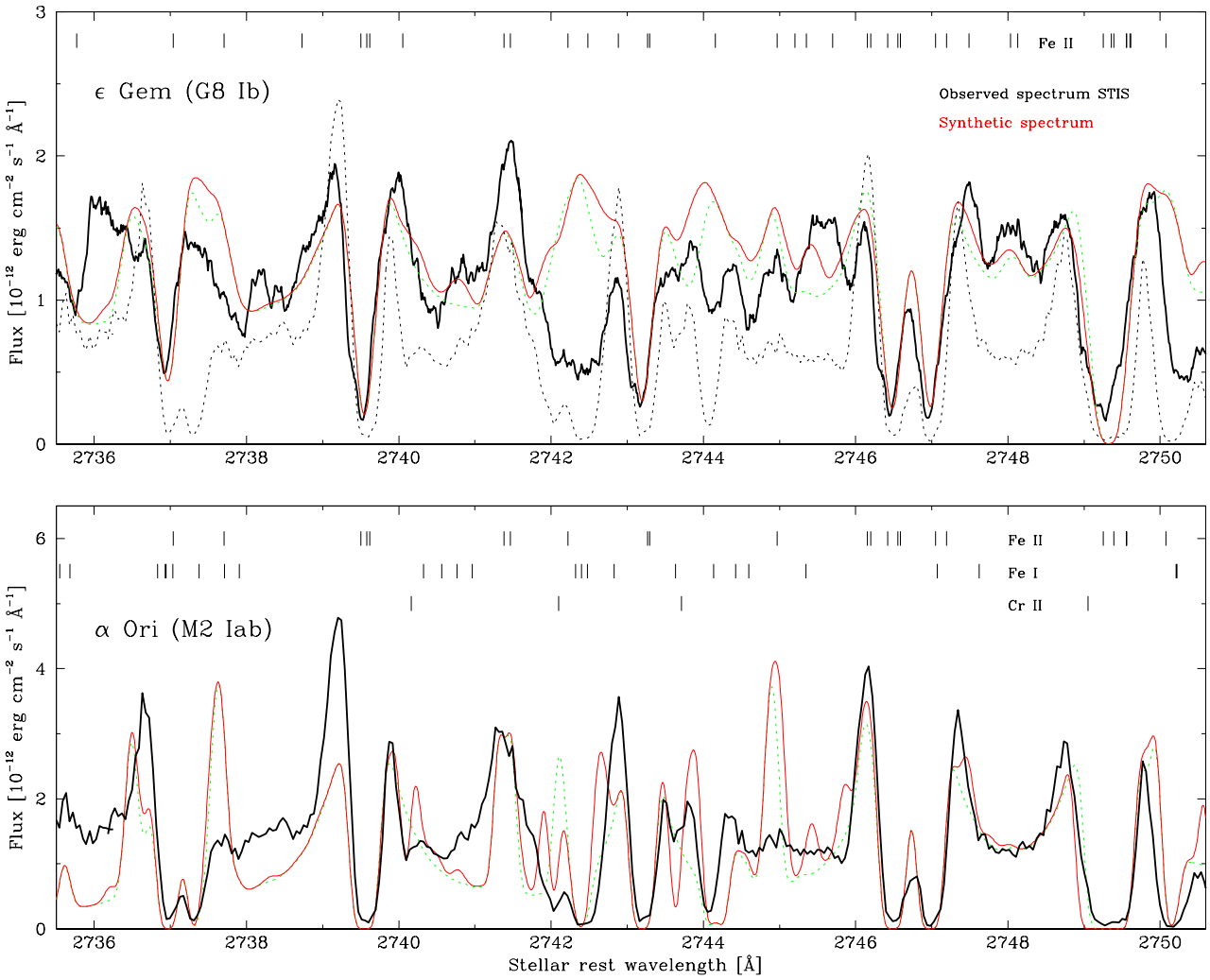
ϵ Gem (G8 Ib)
Observed spectrum STIS
Synthetic spectrum
Fe II
α Ori (M2 Iab)
Fe II
Fe I
Cr II
Flux [10⁻¹² erg cm⁻² s⁻¹ Å⁻¹]
Stellar rest wavelength [Å]
2736
2738
2740
2742
2744
2746
2748
2750

Fig. 1.—

Modeling STIS Spectra

Figure 1 upper panel: A portion of the chromospheric spectrum of the less luminous (Ib) G-type supergiant ϵ Gem, observed with the HST-*Space Telescope Imaging Spectrograph*, is shown by the black solid line. The region between 2736 Å and 2750 Å is typical for its near-UV spectrum, showing many metal emission lines, observed against a UV background continuum. The cores of strong emission lines are *self-absorbed*, producing black troughs with central intensities below the background level. These scattering cores are formed in the upper chromospheric layers, and their shape and Doppler position are determined by the conditions and the velocity field in these layers.

The solid red line shows the synthetic spectrum for this region. The synthesis is performed with a 1D model of the stellar atmosphere. The photospheric model with $T_{\rm eff}$=4250 K and $\log(g)$=1.0 ($R_\star \simeq 140\ R_\odot$) is extended with a semi-empirical model of the chromosphere. The model requires a temperature minimum of ∼3100 K, and a temperature maximum of 7080 K. A LTE synthesis provides good correspondence with the observed spectrum, using the atomic line list available from Kurucz website. The green dotted line shows the synthetic spectrum using only Fe II lines. It reveals that most of the strong features in the near-UV are

blends of Fe II lines, which results from the complex term structure of this ion.

Figure 1 lower panel: A comparison with the STIS spectrum (solid black line) of the M-type supergiant Betelgeuse (Iab) reveals that the chromospheric spectra of both stars are similar (but not identical). The central scattering cores of strong Fe II lines are deeper for Betelgeuse, and often appear intensity saturated, which signals their formation through a much larger column mass. The photospheric model with $T_{\rm eff}$=3500 K and $\log(g)$=−0.5 ($R_\star \simeq 700\ R_\odot$) is extended with a chromosphere with a temperature minimum of 2700 K. The model extends to $\sim$7 $R_\star$, and requires a maximum temperature of 5500 K to provide the best fit (solid red line) with the observed UV spectrum. The green dotted line is computed with Fe I and Fe II lines. The neutral iron lines contribute less in ϵ Gem due to its higher chromospheric temperatures. A number of weak Cr II lines are also identified in Betelgeuse. Note that the model spectrum occasionally produces unobserved intense iron emission lines (i.e. Fe I $\lambda\lambda$2737.633 and Fe II $\lambda\lambda$2744.897). The predicted log(gf)-values of these transitions, with small oscillator strenghts, are overestimated.

Figure 2: The STIS spectrum of ϵ Gem (solid black line) is shown in the stellar rest velocity frame of the Fe II $\lambda\lambda$2739.548 emission line. The synthetic spectrum (solid red line) is computed with a hydrostatic model

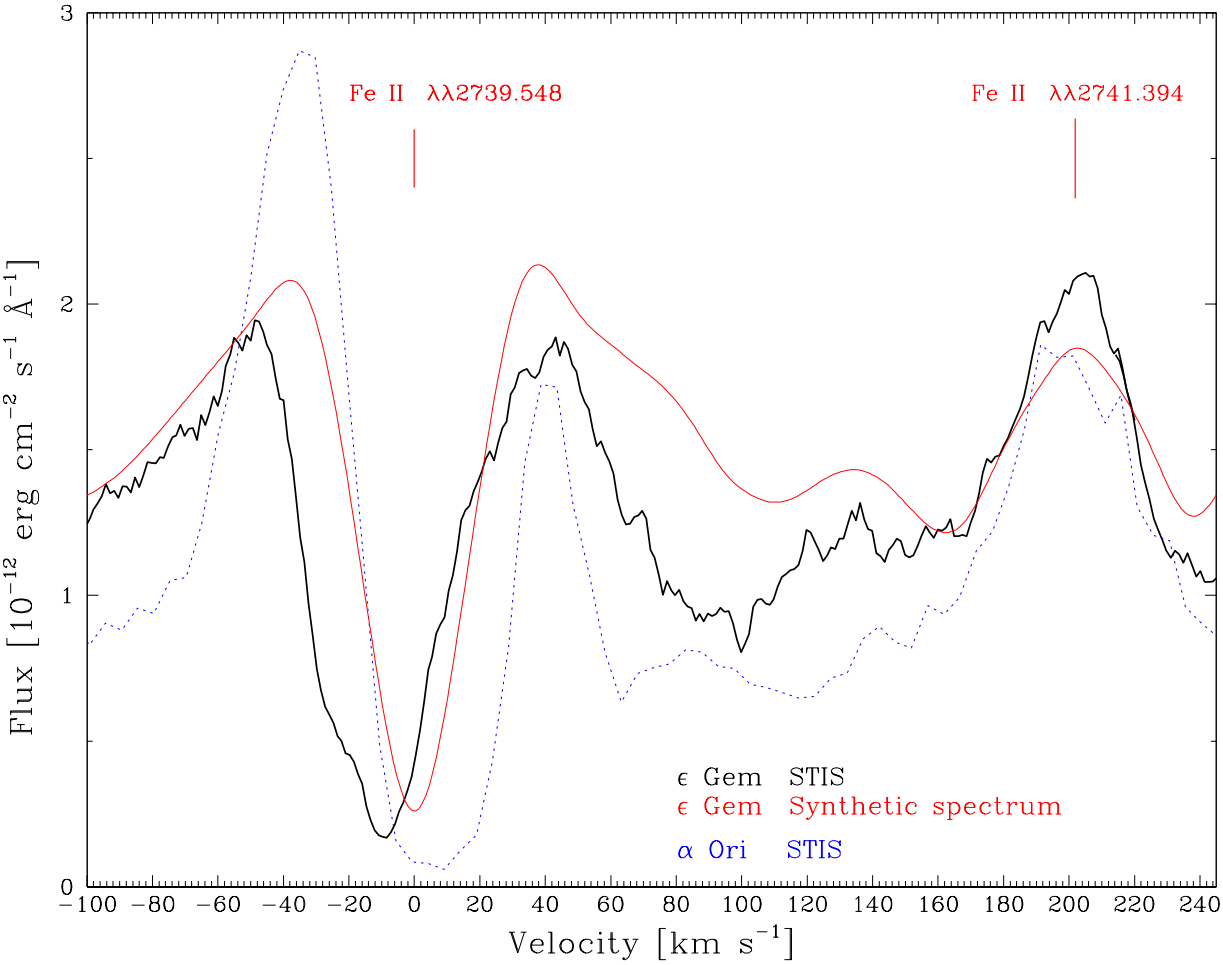
Fe II λλ2739.548
Fe II λλ2741.394
ϵ Gem STIS
ϵ Gem Synthetic spectrum
α Ori STIS
Flux [10^-12 erg cm^-2 s^-1 Å^-1]
Velocity [km s^-1]
0
1
2
3
−100 −80 −60 −40 −20 0 20 40 60 80 100 120 140 160 180 200 220 240

Fig. 2.—

of the chromosphere. It correctly reproduces the equivalent width of the self-absorption core. The Doppler position of the observed core appears however blue-shifted by 5−10 $\mathrm{km\,s^{-1}}$, which indicates expansion in the upper formation layers. The weak emission Fe II $\lambda\lambda$2741.394 line forms closer to the temperature rise, indicating smaller outflow velocities in deeper chromospheric layers. This transition is also an emission line in Betelgeuse (dotted blue line). Co-aligning the emission profiles of this line in both stars reveals that the long-wavelength wing of the self-absorption core is enhanced in Betelgeuse, indicating an average downflow. This is also noticeable for many other self-reversed Fe II lines in the panel above. A detailed modeling of chromospheric down- and upflow, observed with STIS for Betelgeuse between 1998 Jan. and 1999 March, is discussed in Lobel & Dupree (ApJ, 2000, 545, 454).

Figure 3: A comparison of high-resolution (R=114,000) STIS profiles of the Mg II resonance doublet in both stars shows that the scattering cores of the h and k lines are strongly intensity saturated. The remarkable asymmetry of intensity for the emission line components in Betelgeuse is not observed in ϵ Gem. The lines are also narrower for the latter. The Mg II asymmetry in Betelgeuse is explained by blends of self-absorbed *chromospheric* Mn I lines, which scatter part of the blue component of the k line, but enhance the emission in the blue component of the h

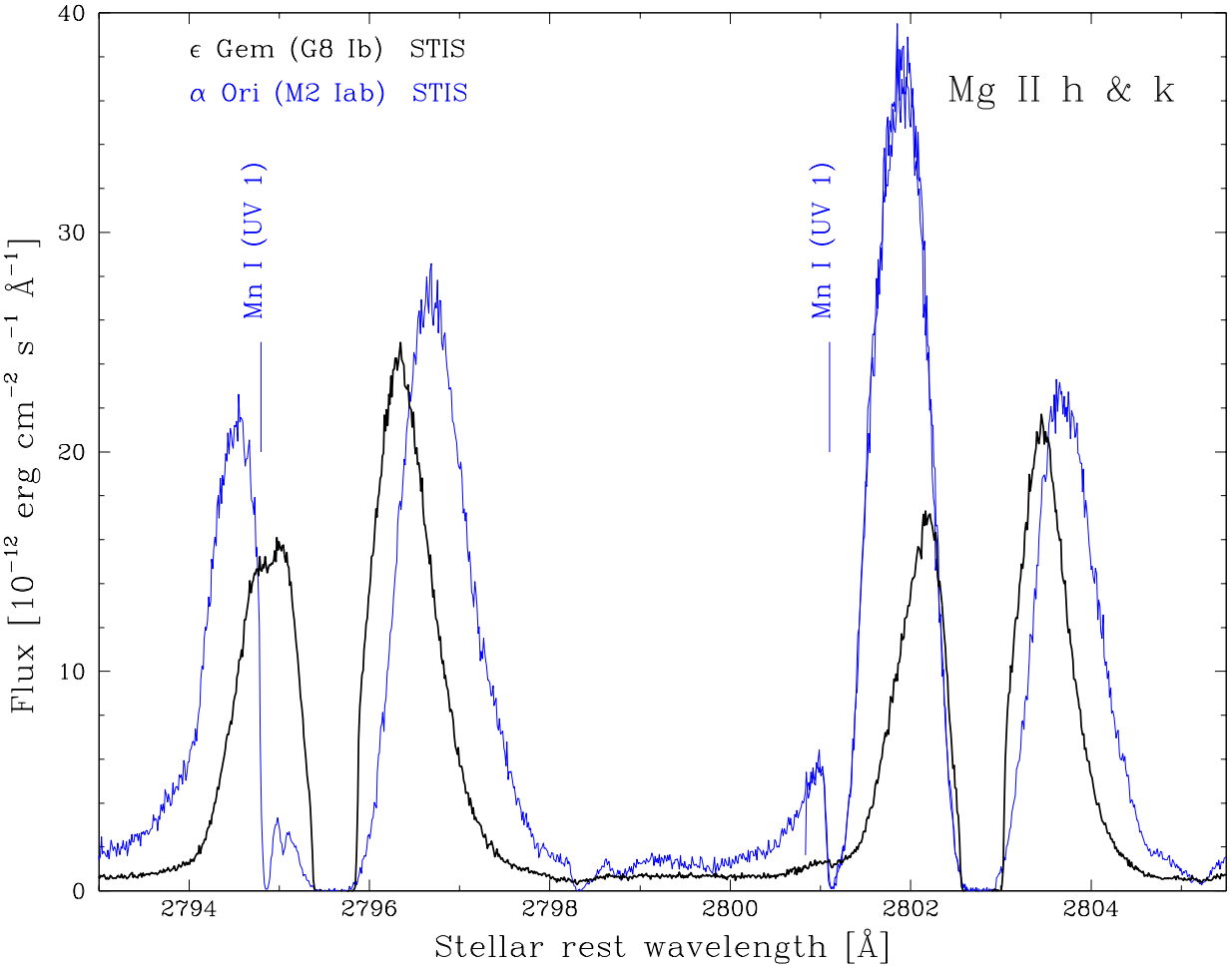
ϵ Gem (G8 Ib) STIS
α Ori (M2 Iab) STIS
Mg II h & k
Mn I (UV 1)
Mn I (UV 1)
Flux [10^-12 erg cm^-2 s^-1 Å^-1]
Stellar rest wavelength [Å]
0
10
20
30
40
2794
2796
2798
2800
2802
2804

Fig. 3.—

line. The thinner and warmer chromosphere of ϵ Gem produces weaker Mn I lines, but their presence is discernable in the STIS spectrum. The very broad lines in Betelgeuse are caused by radiative transfer effects in a spherically extended formation region which is highly turbulent. *IUE* observations of ϵ Gem exhibit strong intensity changes in the long-wavelength emission components of the doublet lines (not shown here). These long-period intensity changes are also observed in Betelgeuse with the higher resolutions of *STIS* and HST-*GHRS*. The variability results from changes in the red wing of the broad self-absorption cores in the h and k lines, which reveals that the chromospheres of supergiants are dynamic, and exhibit variable conditions over time.

Modeling Optical Spectra

Figure 4: A comparative study of high-dispersion (R≃50,000) optical *UES* and *So£n* observations (solid black lines) of ϵ Gem (G8 Ib), 9 Peg (G5 Ib), and α Aqr (G2 Ib) shows temperature effects by the chromosphere on the formation of the Balmer lines. The red lines show the spectrum synthesized in LTE for the photospheric conditions. Best fits to photospheric Fe I lines longward of Hα are obtained for respectively $T_{\rm eff}$=4250 K, 4750 K, and 5250 K, utilizing log(g)=1.0. We find that an accurate LTE synthesis of the photospheric spectrum cannot match the shape and equivalent width of the Hα line. This difference increases towards lower $T_{\rm eff}$, because chromospheric excitation of Hα enhances *relatively* with respect to photospheric excitation. The broad photospheric damping wings in α Aqr decrease towards lower $T_{\rm eff}$, and become very weak in ϵ Gem. The photospheric core contribution also diminishes, and the broadening does not match the observed width. The normalized core depth is computed by ∼0.3 too weak in ϵ Gem. In Betelgeuse ($T_{\rm eff}$=3500 K) the Hα core, computed without the chromosphere, is invisible against the TiO background. Higher chromospheric temperatures are required to populate this transition adequately. The blue line shows the Hα profile computed in NLTE

by means of a spherical model of its chromosphere, which also fits the STIS spectrum in the lower panel of the first graph. The Hα fit requires microturbulence values which increase from 2 ± 1 km s^{-1} in the photosphere, to highly supersonic values in the chromosphere. Similar detailed Hα modeling of the chromospheric conditions of Ib G-supergiants is underway.

Figure 5: The Hβ line reveals a dependence on chromospheric excitation similar to Hα. Photospheric excitation (red lines) does not reproduce the observed profiles (black lines), and the normalized core depth and equivalent width decrease towards smaller $T_{\rm eff}$. The differences of fit become however increasingly smaller for the higher Balmer transitions. These lines mainly form in the deeper photosphere, and require higher excitation temperatures and electron densities. For instance, the chromospheric contribution to Hδ in α Aqr ($T_{\rm eff}$=5250 K) becomes relatively very small, although the chromospheric temperature exceeds $T_{\rm eff}$. The line wings display a strong damping profile which is log(g)-dependent, and which invalidates the determination of chromospheric conditions from this core.

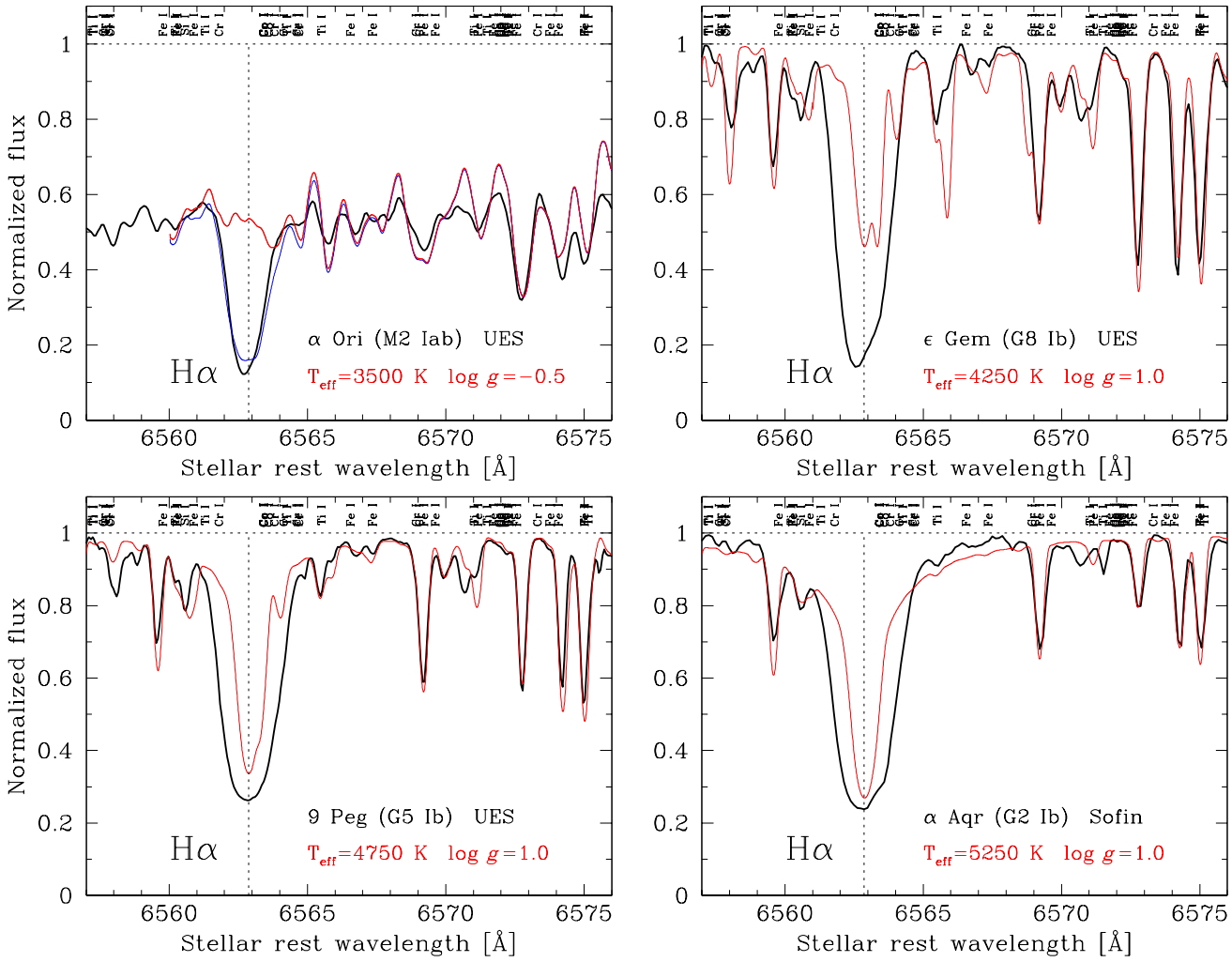
Normalized flux
Stellar rest wavelength [Å]
Hα
α Ori (M2 Iab) UES
T_eff=3500 K log g=−0.5
ϵ Gem (G8 Ib) UES
T_eff=4250 K log g=1.0
9 Peg (G5 Ib) UES
T_eff=4750 K log g=1.0
α Aqr (G2 Ib) Sofin
T_eff=5250 K log g=1.0

Fig. 4.—

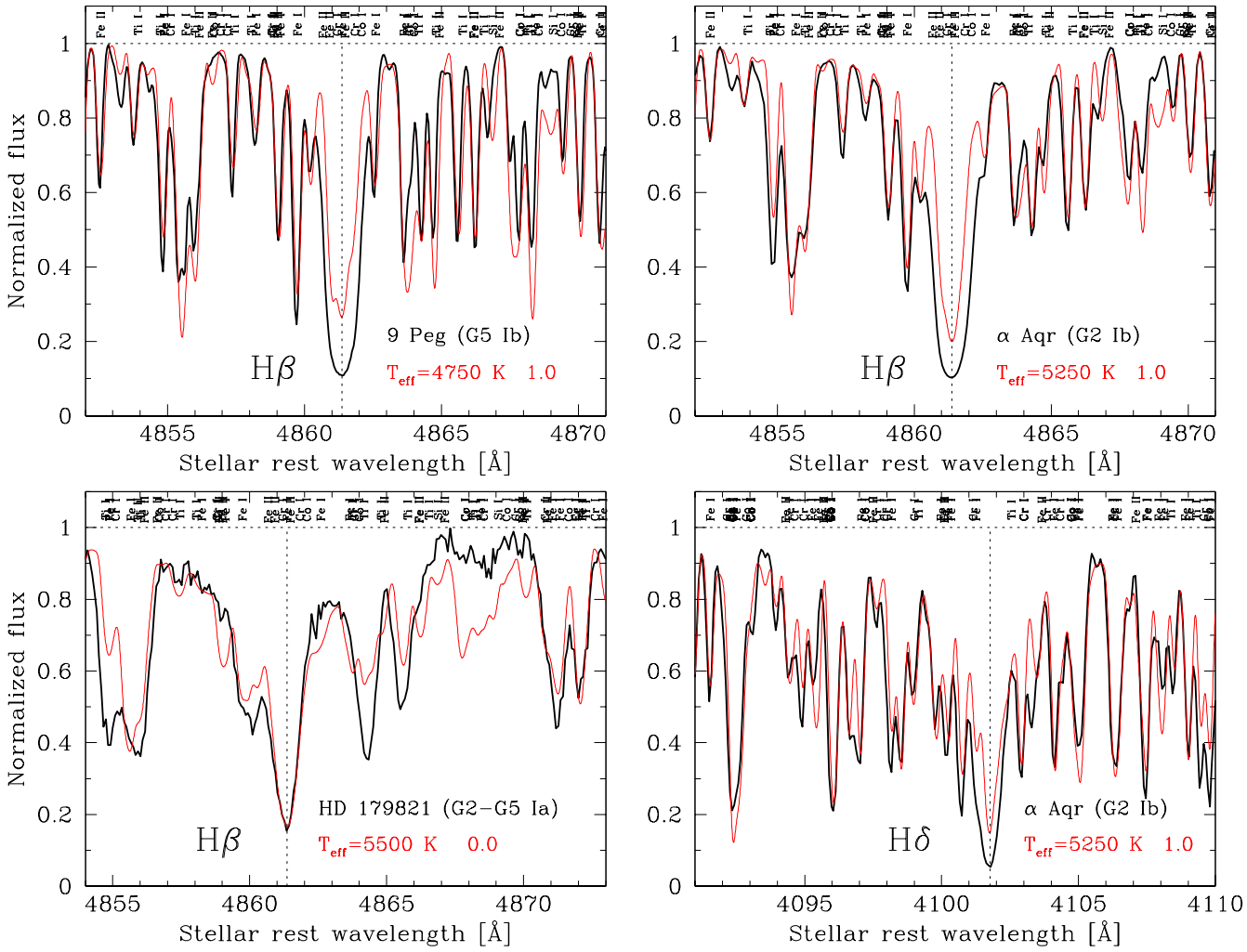
Normalized flux
Stellar rest wavelength [Å]
9 Peg (G5 Ib)
Hβ
T_eff=4750 K 1.0
α Aqr (G2 Ib)
Hβ
T_eff=5250 K 1.0
HD 179821 (G2−G5 Ia)
Hβ
T_eff=5500 K 0.0
α Aqr (G2 Ib)
Hδ
T_eff=5250 K 1.0

Fig. 5.—

Ia vs. Ib G-type Supergiants

A study of Balmer lines in the luminous G-supergiant HD 179821 (Ia) reveals similar Voigt shapes for the Hβ and Hδ lines. We find that $T_{\rm eff}\simeq$5500 K and small $\log(g)\leq$0.0, closely match both line profiles. Higher $T_{\rm eff}$-values produce too broad damping wings. A very large macro-broadening of 20 km s^{-1} is required to fit the shape of ***photospheric*** absorption lines, also observed in other cool Ia super- and hypergiants (e.g. ρ Cas and HR 8752). The Ib-supergiants require smaller macroturbulence values of $\sim$12 km s^{-1}, as for Betelgeuse (Iab). For supergiants, these supersonic values do not result from rapid rotation, but are caused by large-scale atmospheric motion fields. A large macrobroadening is also required to fit the shape of ***chromospheric*** emission lines in STIS spectra of ϵ Gem. Spatially resolved STIS observations of Betelgeuse's chromosphere further reveal a large and isotropic macrobroadening of 9 ± 1 km s^{-1} (Lobel & Dupree, 2001, ApJ), which suggests a uniform distribution of large-scale turbulence in the chromospheres of Iab$-$Ib supergiants.

Figure 6: HD 179821 has recently been proposed as a low-mass post-AGB candidate, based on a LTE abundance analysis by Thévenin et al. (A&A 2000, 359, 138). The far-IR excess indicates a cool detached

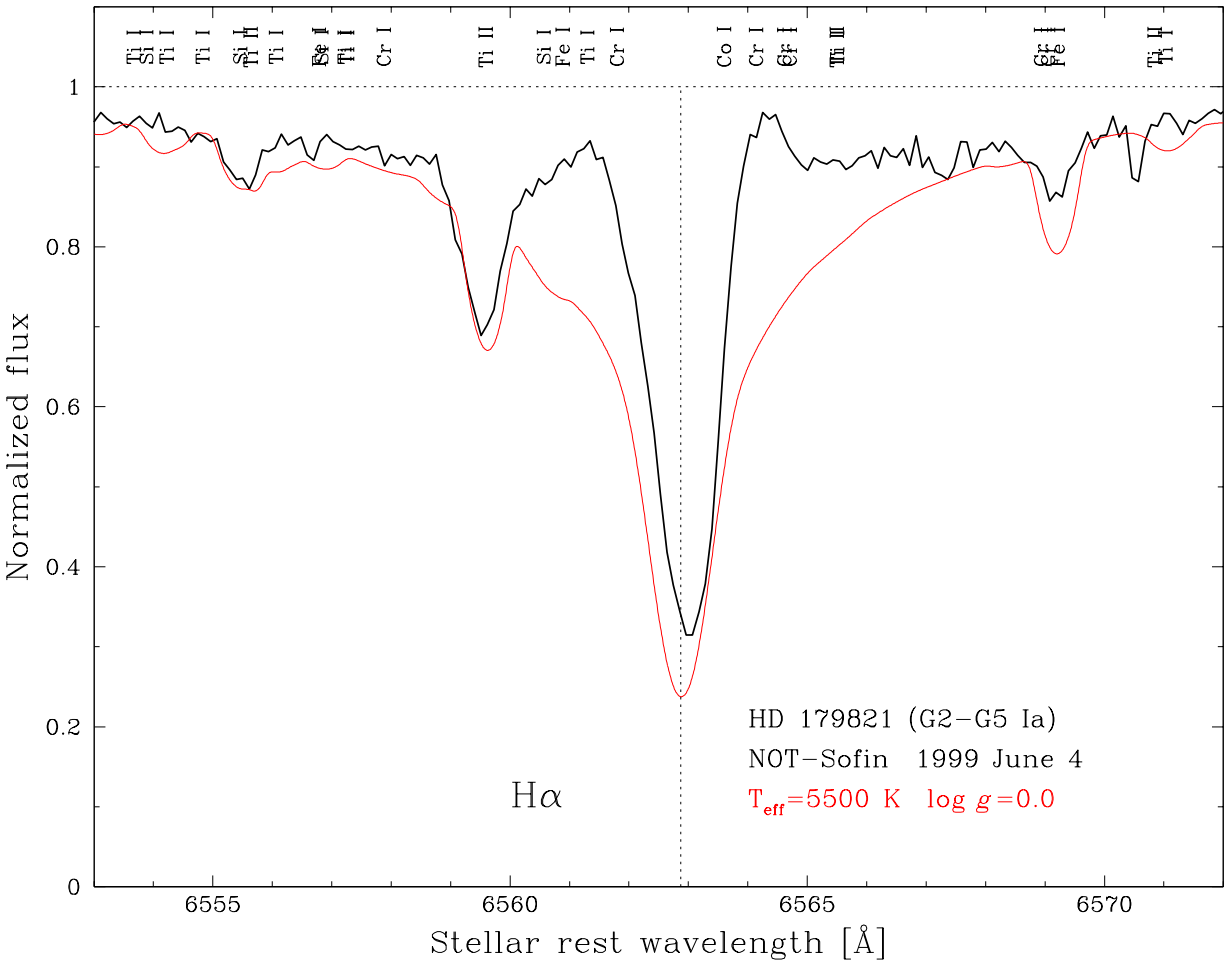
Ti I
Si I
Ti I
Ti I
Si I
Ti I
Ti I
Fe I
Ti I
Cr I
Ti II
Si I
Fe I
Ti I
Cr I
Co I
Cr I
Cr I
Ti II
Ca I
Fe I
Ti I
Ti I
Normalized flux
1
0.8
0.6
0.4
0.2
0
6555
6560
6565
6570
Stellar rest wavelength [Å]
Hα
HD 179821 (G2−G5 Ia)
NOT−Sofin 1999 June 4
T_eff=5500 K log g=0.0

Fig. 6.—

dust shell. There is however no consensus on the evolutionary status of this supergiant. Its high expansion velocity of 34 $\mathrm{km\,s^{-1}}$ is much larger than the value of 10−15 $\mathrm{km\,s^{-1}}$ for low-mass post-AGB stars, which suggests a massive supergiant. Our Hα observations (black line), reveal variable red- and blueshifted emission, with respect to the line profile computed in LTE (red line). These emission humps result from NLTE-effects in a fast and spherically expanding wind, inside the dust cavity. They sporadically appear above the continuum level, which is also observed for the very luminous hypergiant ρ Cas (F2-G Ia$^+$) (Lobel, 1997, PhD thesis).

Figure 7: Further spectral indications for the very small gravity acceleration of HD 179821, typical for massive Ia-supergiants, is obtained from Ca II K (black line). The prominent central emission of Ib-supergiants (i.e. for α Aqr with $\log(g)\simeq1.0$; blue line), is not observed. It indicates the absence of a 'classic' chromosphere for HD 179821, with excitation temperatures below $T_{\rm eff}$. Our observations of ρ Cas (with $M_\star$=20−40 $M_\odot$ and $\log(g)\simeq0.0$) reveal no central emission in the Ca II H & K lines.

This introductory study of the chromospheres of Ib-supergiants serves to develop semi-empiric dynamic models of the outer atmospheric structure,

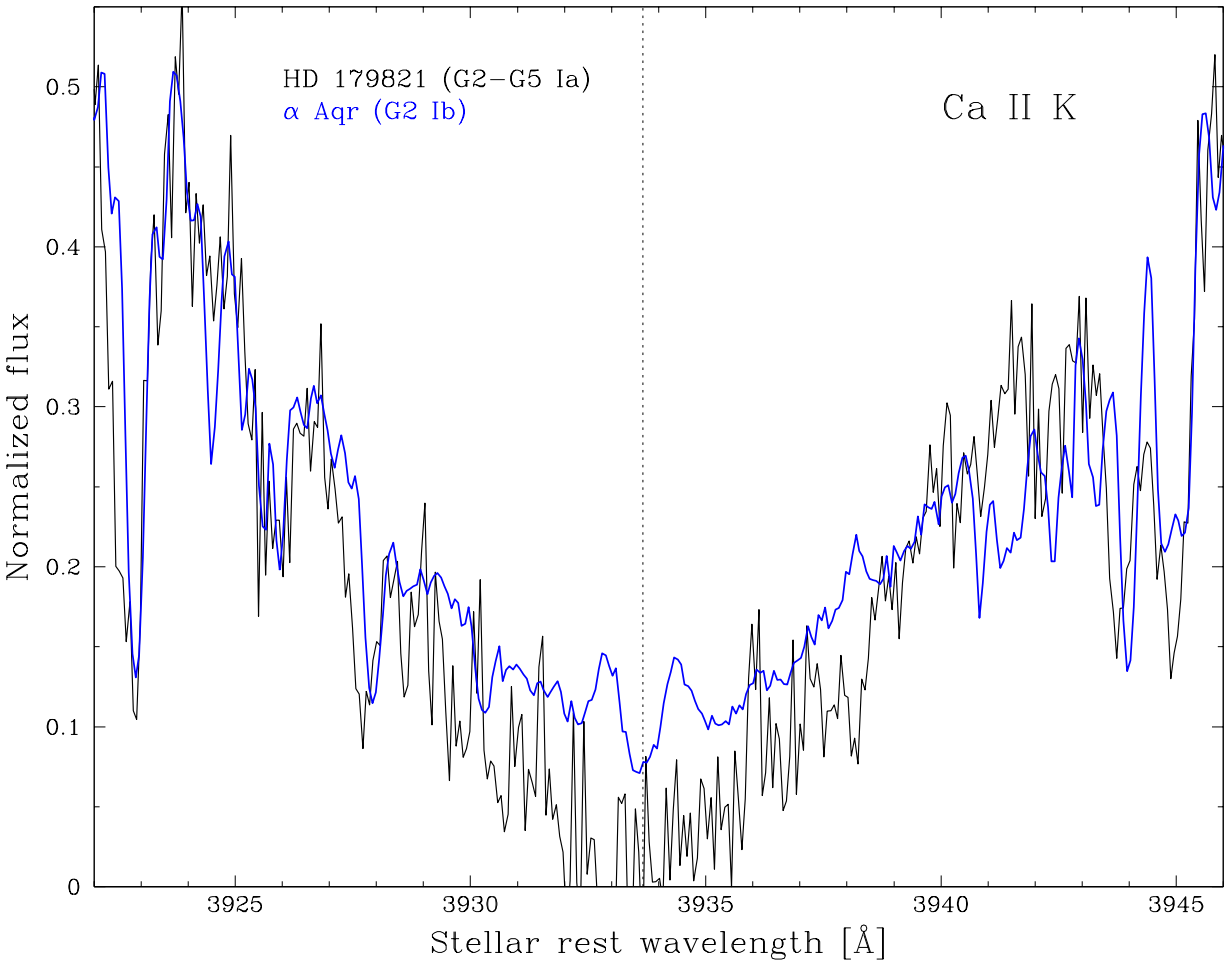
HD 179821 (G2−G5 Ia)
α Aqr (G2 Ib)
Ca II K
Normalized flux
0
0.1
0.2
0.3
0.4
0.5
3925
3930
3935
3940
3945
Stellar rest wavelength [Å]

Fig. 7.—

based on far-UV high-temperature indicators such as C IV, Si IV, and O VI lines, observed in their STIS and FUSE spectra.